Adv Polym Sci (2018) 281: 79–104
DOI: 10.1007/12_2017_9

Published online: 30 April 2017

The Generalized Stability Model and Its Applications in Polymer Colloids

Hua Wu, Dan Wei, and Massimo Morbidelli

Abstract This chapter reviews the generalized stability model developed in recent years Jia et al. (J. Colloid Interface Sci. 302:187–202, 2006) and its application to different polymer colloids. The most important feature of this model is that it accounts simultaneously for the interplay between different physicochemical processes, such as surfactant adsorption equilibrium on the particle surface, association equilibria of surface charges with counterions involved in the system, and DLVO and non-DLVO colloidal interactions. Through its application to different polymer colloids produced from industrial polymerization processes, we demonstrate that the generalized stability model is powerful and capable of describing the stability of the most complicated colloidal systems. After the model has been established, it can be used to analyze how the interplay of the relevant processes affects the stability of colloids, which is not often feasible through experimental investigation.

Keywords Colloidal interaction • Counterion association • Fuchs stability ratio • Physicochemical process interplay • Stability model • Surfactant adsorption

H. Wu (✉) and M. Morbidelli (✉)
Department of Chemistry and Applied Biosciences, ETH Zurich, Institute for Chemical and Bioengineering, 8093 Zurich, Switzerland
e-mail: hua.wu@chem.ethz.ch; massimo.morbidelli@chem.ethz.ch

D. Wei
School of Chemistry and Chemical Engineering, Guangdong Pharmaceutical University, 528458 Zhongshan, Guangdong, China

Contents

1 Introduction

Latexes produced by emulsion polymerization are typical colloids, stabilized through adsorption of ionic surfactants on the particle surface. The electrical charges generate an electrical double layer (EDL), leading to electrostatic repulsion, which, when prevailing over the short-range van der Waals attraction, results in a repulsive barrier that kinetically stabilizes the particles. Quantification and control of the stability of polymer colloids are of great importance in industrial practice. Thus, it is essential to develop a stability model that can describe the stability of industrial polymer colloids, accounting for the effect of operating variables (e.g., type and concentration of electrolyte, system pH, etc.) on the stability.

The dominant theoretical studies describing colloidal stability focus on how to correctly describe colloidal interactions, but the effect on colloidal stability of interplay between various physicochemical processes is seldom accounted for. The centerpiece in describing colloidal interactions is the DLVO (Deryaguin–Landau–Verwey–Overbeek) theory [1, 2], which models the competition between van der Waals attraction and EDL repulsion. Additional non-DLVO forces (e.g., long-range dispersion forces, short-range hydration forces, steric forces, capillary condensation) are known to be important under specific conditions [3–7], but, unlike DLVO forces, such non-DLVO forces are difficult to measure experimentally or predict theoretically, particularly for industrial polymer colloids.

In practical applications, for a chosen colloid, one often first measures the surface charge or zeta-potential under well-defined conditions, and then uses the measured surface charge or potential in the DLVO model (accounting for the ionic strength) to compute the interaction energy barrier or the Fuchs stability ratio, W. Although this method can model the stability of a specific colloid under specific conditions (i.e., ionic strength, ion types, particle concentration, etc.), it cannot be applied to describe the stability of the same colloid at different ionic strengths, ion types, and particle concentrations by simply changing the ionic strength and ion valence in the DLVO model. This is because the above approach ignores the interplay between the various physicochemical processes (e.g., colloidal

interactions, counterion association equilibrium, surfactant adsorption equilibrium). As a result of such interplay, changes in the ionic strength and type lead to changes in the counterion association equilibria, and thus to changes in the surface charge and potential. Consequently, there are changes in the ion and surfactant distributions (the Boltzmann effect), thus coupled back with further changes in counterion association. The interplay becomes even more complex for industrial polymer colloids, where the surfactant systems are often very complex.

To account for the interplay mentioned above, our group has developed a generalized stability model to describe colloidal stability [8], where different physicochemical processes, such as surfactant adsorption equilibrium, counterion association equilibria, and DLVO and non-DLVO colloidal interactions, have been integrated in a single model so that their coupled interplays can be simultaneously accounted for and correctly described. In this review, we first briefly describe the developed generalized stability model and then discuss its successful application in modeling the stability of different polymer colloids.

2 The Generalized Stability Model

The interactions between charged particles and electrolytes in solution lead to ion distributions around the particles, which are governed by the Poisson–Boltzmann equation. When the ionic strength of the system is changed, redistribution of the ionic species occurs, leading to changes in the association equilibria between the ionic surfactant adsorbed on the particle surface and the counterions in the disperse medium. Consequently, this leads to changes in the surface charge density and colloidal stability. Here, we briefly describe how the generalized stability model accounts simultaneously for different processes, based on the theories available in the literature [2, 9–11].

2.1 Surfactant Adsorption Equilibrium

Ionic surfactants (denoted by E in the following) are commonly used in emulsion polymerization. They are adsorbed on the particle surface and their dissociation forms charges on the surface, stabilizing the particle. The charges generated from the surfactant molecules are referred to as mobile charges because of the reversibility of surfactant adsorption. As an equilibrium process, surfactant adsorption depends on the surfactant concentration in the disperse medium. Different adsorption isotherms are proposed in the literature to describe surfactant adsorption [12, 13], depending on the nature of the particle surface and surfactant type. The Langmuir-type adsorption isotherm is simple and probably the most commonly used:

$$bC_t^i = \frac{\Gamma/\Gamma_\infty}{1 - \Gamma/\Gamma_\infty} \tag{1}$$

where Γ is the surfactant surface coverage, Γ_∞ at saturation, and b the adsorption constant. It is particularly worth noting that C_t^i is the total surfactant concentration at the particle–liquid interface, which is different from the concentration in the bulk disperse medium, C_t^b.

On the particle surface there are also ionically dissociable polymer end groups, such as the sulfate head groups ($-SO_4^-$) from the initiator and potassium persulfate (KPS). These charges are covalently bound to the surface; they are denoted by L and referred to as fixed charges in t.

2.2 Electrolyte Dissociation Equilibrium

Apart from the ionic surfactant, different electrolytes may exist in polymer colloids. Thus, their dissociation equilibria should be taken into account. It should be pointed out that for each electrolyte, there are two different dissociation equilibria: one at the particle–liquid interface and another in the bulk disperse medium. The properties of the particle surface are computed on the basis of the equilibria at the particle–liquid interface, instead of the properties in the bulk disperse medium. This is one of the essential features of the generalized stability model.

In the description of the dissociation equilibria, we use E^- and L^- to denote the surfactant and fixed charge anions, M_m^+ and M_d^{2+} for the mono- and divalent cations, A_m^- and A_d^{2-} for the mono- and divalent anions, and H^+ for the proton. The divalent cation M_d^{2+} is assumed to combine with E^- and L^- only in the form of 1:1 complexes, M_dE^+ and M_dL^+. This assumption is reasonable at the interface for aliphatic surfactants [11], because 1:2 complexes can be formed only when the surfactant hydrocarbon chains are oriented perpendicular to each other, facing the metal ions with their functional groups. Except for cases of extremely low surface coverage, this is not a preferred conformation for surfactant molecules adsorbed on a particle surface [14]. The association of M_d^{2+} with A_d^{2-} is also included, but all the weak associations of M_m^+ with anions, A_m^- and/or A_d^{2-}, are ignored. The associations of H^+ with both A_m^- and A_d^{2-} are accounted for to correctly predict the system pH. These associations are particularly important when carboxyl groups are the main source of the surface charges, which are very sensitive to the system pH. For the association between H^+ with A_d^{2-}, we consider only 1:1 association and the very weak 2:1 association is ignored. Note that all these assumptions are not strictly needed for the generalized stability model, and are only proposed treatments based on some general validity in the literature. In addition, we generally assume that the equilibrium constant K is independent of whether the association occurs at the interface or in the bulk disperse medium. The acidic surfactant, HE, is assumed to be water-soluble, regardless of whether it is associated or dissociated.

It should be pointed out that when both cationic surfactant and cationic fixed charges, E^+ and L^+, are used, one should consider their associations with anions in the disperse medium. However, in the specific case of cationic surfactant and

anionic fixed charges, the applied surfactant first neutralizes the negative fixed charges. Beyond the charge compensation point, the particle surface progressively becomes positively charged [15]. In this case, such charge compensation has to be included in the electrolyte association equilibria.

2.3 Colloidal Interactions

The classical DLVO model accounting for electrostatic repulsive (U_R) and van der Waals attractive (U_A) potentials is considered here. As indicated by various studies [4, 6, 7, 16–19], in many polymer colloids there is often an additional short-range repulsive force that decays exponentially with distance. This force exhibits a specific electrolyte ion effect, which is related to the hydration strength of the ions, and this non-DLVO force is often referred to as "hydration force." Thus, in addition to the DLVO interactions, we generally include this non-DLVO hydration force, referred to as the hydration interaction, U_{hyd}. Thus, the total interaction energy U is given as follows:

$$U = U_A + U_R + U_{hyd} \tag{2}$$

where the van der Waals attraction, U_A, is computed with the Hamaker relation [1]:

$$U_A = -\frac{A_H}{6}\left[\frac{2}{l^2-4} + \frac{2}{l^2} + \ln\left(1 - \frac{4}{l^2}\right)\right] \tag{3}$$

where A_H is the Hamaker constant and $l = r/a$, where r is the center-to-center distance between two particles and a is the particle radius. For the electrostatic repulsion, U_R, we use the modified Hogg–Healy–Fuersteneau expression [20]:

$$U_R = \frac{4\pi\varepsilon_0\varepsilon_r a\psi_0^2}{l} \ln\{1 + \exp[-\kappa a(l-2)]\} \tag{4}$$

where ε_0 is the vacuum permittivity, ε_r the relative dielectric constant of the medium, and ψ_0 the surface potential. The Debye–Hückel parameter κ is given by:

$$\kappa = \sqrt{\left(e^2 N_A \sum_j z_j^2 C_j^b\right) \Big/ (\varepsilon_0\varepsilon_r kT)} \tag{5}$$

with e being the electron charge, N_A the Avogadro constant, C_j^b and z_j the concentration and charge valence of the j-th ion in the bulk disperse medium, respectively; k is the Boltzmann constant and T the absolute temperature. The hydration force is modeled with an exponential decay function [9, 21]:

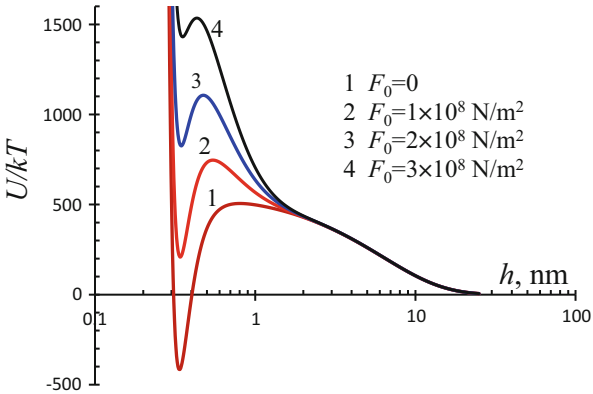

Fig. 1 Example of the typical effect of the presence of the hydration interaction on the total interaction energy [23]

$$F_{\text{hyd}} = F_0 \exp(-h/\delta_0) \tag{6}$$

where $h = r - 2a$ is the surface-to-surface distance between particles, F_0 is the hydration force constant, and δ_0 is the characteristic decay length. Applying the Deryaguin approximation leads to the corresponding hydration interaction energy between two spherical particles [22]:

$$U_{\text{hyd}} = \pi a F_0 \delta_0^2 \exp(-h/\delta_0) \tag{7}$$

Typical examples of the total interaction profiles in the presence of the hydration interaction are shown in Fig. 1 (cases 2, 3, and 4) and compared with the case in the absence of hydration (case 1). It can be seen that the hydration interaction not only increases the interaction barrier but also moves the primary minimum upward.

With the above total interaction energy U, one can compute the Fuchs stability ratio, W, based on its definition [24]:

$$W = 2 \int_2^\infty \frac{\exp(U/kT)}{Gl^2} \mathrm{d}l \tag{8}$$

where G is a hydrodynamic function accounting for additional resistance caused by squeezing of the fluid during the approach of a particle [25]:

$$G = \frac{6l^2 - 20l + 16}{6l^2 - 11l} \tag{9}$$

2.4 Computation of Key Quantities of the Generalized Stability Model

One of the most important quantities related to the processes described above is the total effective charge density on the particle surface, with which one can directly compute the surface potential needed in colloidal interactions. As mentioned previously, there are two types of charge, mobile and fixed. Of the adsorbed species on the particle surface, HE, M_mE, M_dE^+, and E^-, only the last two contribute to the surface charge. The net mobile charge density coming from the adsorbed surfactants, $\sigma_{0,E}$, is given by:

$$\sigma_{0,E} = F\left(C^S_{M_dE^+} - C^S_{E^-}\right)\frac{V_p}{A_p} = \frac{aF}{3}\left(K_{M_dE}C^i_{M_d^{2+}} - 1\right)C^S_{E^-} \tag{10}$$

where the superscripts s and i denote quantities on the particle surface and at the interface, respectively. F is the Faraday constant and V_p and A_p are the volume and surface area of a particle, respectively. Note that the sign of the mobile charge density given by Eq. 10 depends on the difference in the concentrations of M_dE^+ and E^- on the surface. When the association between E^- and M_d^{2+} is very strong, or when the M_d^{2+} concentration in the bulk disperse medium is substantially high, the net mobile charge on the surface is positive and charge sign inversion occurs. The charge sign inversion is often used to explain the re-stabilization phenomenon observed at substantially high concentrations of divalent cation in the liquid phase [26–29].

For the net fixed charge, we can similarly write:

$$\sigma_{0,L} = \frac{aF}{3}\left(C^S_{M_dL^+} - C^S_{L^-}\right) = \frac{aF}{3}\left(K_{M_dL}C^i_{M_d^{2+}} - 1\right)C^S_{L^-} \tag{11}$$

Therefore, the total surface charge density, σ_0, is given by:

$$\sigma_0 = \sigma_{0,E} + \sigma_{0,L} \tag{12}$$

It should be noted again that the above equations for computation of charge are valid only when both the mobile and fixed charges are negative. When the mobile and/or fixed charges are positive, the above equations must be modified accordingly.

As mentioned above, the distribution of all the ionic species in the system is described by the Poisson–Boltzmann equation. For simplification of the description, we treat it in the frame of the classical Gouy–Chapman theory [2, 11]. Thus, we obtain the following expression to correlate between the surface charge density, σ_0, the surface potential, ψ_0, and the ionic strength in the bulk disperse medium, C_j^b:

$$\sigma_0 = -\left\{R_0 \sum C_j^b \left[\exp\left(-\frac{z_j e\psi_0}{kT}\right) - 1\right]\right\}^{1/2} \tag{13}$$

where $R_0 = 2F\varepsilon_0\varepsilon_r kT/e$.

The other important quantities to be properly computed are the mass balances of each species distributed in the different phases. Let us use $C_{j,0}$ to represent the concentration of the j-th species initially added to the system. It is distributed on the particle surface and in the disperse medium at equilibrium according to:

$$C_{j,0} = \phi C_j^S + N_0 \int_0^{V_{l,p}} C_j(x)\mathrm{d}V(x) \tag{14}$$

where ϕ is the particle volume fraction, N_0 the particle number concentration, and $V_{l,p}$ the liquid volume that on average can be assigned to each particle ($V_{l,p} = 1/N_0$). The first term on the right-hand side of Eq. (14) is the mass on the particle surface, and the second is the mass distributed in the entire disperse medium, which can be divided into two regions, the diffuse layer near the particle surface and the bulk disperse medium:

$$\begin{aligned} \int_0^{V_{l,p}} C_j(x)\mathrm{d}V(x) &= \int_0^{V_d} C_j^d \mathrm{d}V + \int_0^{V_{l,p}} C_j^b \mathrm{d}V \\ &= \int_0^{V_d} C_j^d \mathrm{d}V + \left(V_{l,p} - V_d\right) C_j^b \end{aligned} \tag{15}$$

where V_d is the liquid volume occupied by the diffuse layer, and C_j^d and C_j^b the concentrations of the j-th component in the diffuse layer and in the bulk disperse medium, respectively. To solve the material balance, it is necessary to estimate V_d. For a moderate or thin EDL (~2 nm) compared with the particle radius ($a > 30$ nm), the contribution of the diffuse layer (i.e., the first term on the right-hand side of Eq. 15) to the total material balance is relatively small, and the concentration in the diffuse layer can be simply replaced by the concentration in the bulk disperse medium (i.e., $C_j^d \approx C_j^b$), which should not result in significant error in the material balance. In this way, Eq. 14 reduces to:

$$C_{j,0} = \phi C_j^S + (1 - \phi) C_j^b \tag{16}$$

Note that such an approximation is only for the purpose of the material balance computation and is not applied in the calculation of association equilibria and surface charge density.

Therefore, in summary, once the surfactant adsorption parameters in Eq. (1) and all the electrolyte association constants are known, the set of equations described in Sect. 2 can be solved simultaneously to obtain the surface potential or charge density, the concentrations of all species on the particle surface and in the bulk disperse medium, and finally the Fuchs stability ratio W.

3 Applications of the Generalized Stability Model

To demonstrate the reliability of the generalized stability model, we have applied it to various polymer colloids stabilized in one of three ways: by purely mobile charges, by purely fixed charges, or by both mobile and fixed charges. The unknown model parameters were estimated using a few values of the Fuchs stability ratio, W, as determined experimentally for various salt types and concentrations. Application of the model allows one to monitor the dynamics of surfactant partitioning between particle surface and disperse medium, analyze the variation in surface charge density and potential as a function of the electrolyte type and concentration, and predict the critical coagulant concentration (CCC) for fast coagulation, which can be defined as the minimum coagulant (salt) concentration at which no repulsive barrier exists between colloidal particles.

3.1 Fluorinated Elastomer Latex with Only Mobile Charges [8]

The first polymer colloid used to demonstrate the feasibility of the generalized stability model was a fluorinated elastomer latex, manufactured by Solvay (Italy) through emulsion polymerization. This colloid does not have fixed charges and is stabilized purely by the surfactant (E), a perfluoropolyether (PFPE)-based carboxylate. The particle radius is 60 nm, the surfactant concentration is 33.3 mol/m^3 polymer, and the surfactant counterion is Na^+. The original latex is acidic due to the presence of a small amount of HF, whose concentration at the particle volume fraction $\phi = 5.0 \times 10^{-3}$ is equal to 1.6×10^{-3} mol/L.

3.1.1 Estimation of the Model Parameters

Application of the model involves knowing various parameters. Some can be found in the literature, but others have to be determined experimentally. The proposed approach is first to experimentally measure a few W values with different types of salts and then fit these data with the generalized stability model to obtain the unknown parameters. Figure 2 reproduces some W values measured using

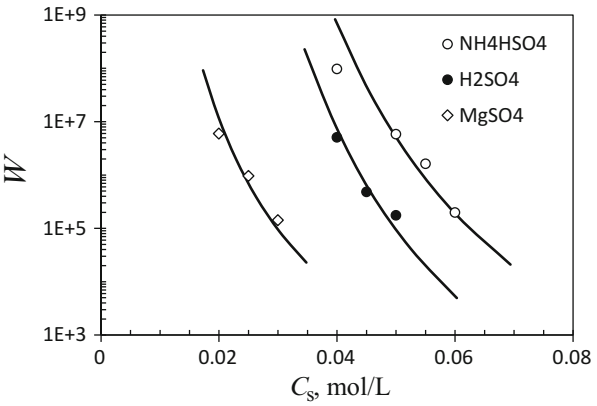

Fig. 2 Values of the Fuchs stability ratio (W) of a fluorinated elastomer latex measured as a function of the salt concentration, for three types of salt, NH_4HSO_4, H_2SO_4, and $MgSO_4$, at $\phi = 5.0 \times 10^{-3}$. The *solid curves* show fitting of the model [8]

NH_4HSO_4, H_2SO_4, and $MgSO_4$. The details of how to measure W values can be found in the original paper [8].

Let us first consider the cases using H_2SO_4 and NH_4HSO_4, both of which involve generation of protons in the solution that can associate with the carboxyl groups of E. There are two parameters (K_{HE} and $K_{HSO_4^-}$) for the associations of H^+ with the surfactant E and the anion SO_4^{2-}, respectively:

$$H^+ + E^- \rightleftarrows HE \quad K_{HE} = C_{HE}/(C_{H^+} + C_{E^-}) \tag{17}$$

$$H^+ + SO_4^{2-} \rightleftarrows HSO_4^- \quad K_{HSO_4^-} = C_{HSO_4^-}/\left(C_{H^+} + C_{SO_4^{2-}}\right) \tag{18}$$

The $K_{HSO_4^-}$ value can be found in the literature and is equal to 97.0 L/mol [30]. There is also the constant, K_{NH_4E}, for the association of NH_4^+ with E:

$$NH_4^+ + E^- \rightleftarrows NH_4E \quad K_{NH_4E} = C_{NH_4E}/\left(C_{NH_4^+} + C_{E^-}\right) \tag{19}$$

The associations of NH_4^+ with the other anions are known to be very weak and can be ignored [31]. Thus, for H_2SO_4 and NH_4HSO_4, two association parameters K_{HE} and K_{NH_4E} need to be estimated.

For the adsorption of surfactant (E) on the particle surface, we consider the Langmuir isotherm (Eq. 1), which involves two parameters, Γ_∞ and b. The saturation coverage (Γ_∞) depends mainly on the affinity between the surfactant and the particle surface but not on the electrolyte. Thus, we take the value $\Gamma_\infty = 5.5 \times 10^{-6}$ mol/m^2, as reported elsewhere [32].

For colloidal interactions, we assume the presence of the hydration interaction, which involves two parameters, F_0 and δ_0 in Eq. (6). Literature information indicates that F_0 lies in the range between 1×10^6 and 5×10^8 N/m^2 and δ_0 in the range between 0.2 and 1.0 nm [33]. We consider here that $\delta_0 = 0.6$ nm, which is approximately twice the size of a water molecule and, instead, F_0 is to be fitted.

Table 1 Values of parameters for the generalized stability model in the case of fluorinated elastomer latex [8]

Parameter		Cation (M)		
		H^+	NH_4^+	Mg^{2+}
Association constants	K_{ME} (L/mol)	29.4[a] (30)	11.2[a]	7.8[a]
	K_{MSO_4} (L/mol)	97.0	–	28.8
Hydration parameters	F_0 (10^6 N/m^2)	1.15[a]	1.25[a]	1.36[a]
	δ_0 (nm)	0.6	0.6	0.6
Adsorption parameters	Γ_∞ (10^{-6} mol/m^2)	5.1 (5.1)		
	b (10^3 L/mol)	3.5[a] (4.0)		

Values in parentheses are taken from the literature
[a]Fitted values

Another interaction parameter, the Hamaker constant, is assumed to be equal to that of a similar fluorinated polymer, PTFE, so that $A_H = 3.0 \times 10^{-21}$ J [34].

Therefore, there are four totally unknown parameters, K_{HE}, K_{NH_4E}, b, and F_0. To obtain these unknown parameters, a proper set of initial values are chosen for each parameter to solve the set of nonlinear algebraic equations, Eqs. 1–16. Then, the best fit is obtained to the measured W values in the cases of H_2SO_4 and NH_4HSO_4, using a proper optimization algorithm. The values of the parameters obtained in the cases of H_2SO_4 and NH_4HSO_4 are given in Table 1, and the good agreement between simulated and experimental W values is shown in Fig. 2.

We next consider the case of $MgSO_4$. The surfactant adsorption parameters obtained previously are still valid. Association of the surfactant with H^+ is also present in this system because the latex is acidic, and the association constant K_{HE} obtained above can be used directly. Thus, there are only two parameters to be determined, the association equilibrium constant, K_{MgE^+}, and the hydration constant, F_0. The result of the fitting is also shown in Fig. 2, and the values of the parameters are reported in Table 1. It is interesting that the association constant of Mg^{2+} is slightly smaller than that of NH_4^+. This could arise from the structure of NH_4^+, which is different from that of the metal cations.

3.1.2 Model Predictions

With all the parameters available in Table 1, one can now use the generalized stability model to predict the desired quantities for the given latex. Let us first apply it to predict the system pH under various conditions, particularly as a function of the salt type and concentration. Figure 3 compares predictions with experimentally measured pH values. It is evident that the model predictions agree excellently with the experiment results in all three cases. In the cases of H_2SO_4 and NH_4HSO_4, because they produce H^+ both measured and predicted values of pH in Fig. 3 decrease as the concentration of H_2SO_4 or NH_4HSO_4 increases. On the other hand, in the case of $MgSO_4$, because the anion SO_4^{2-}, at equilibrium, can consume

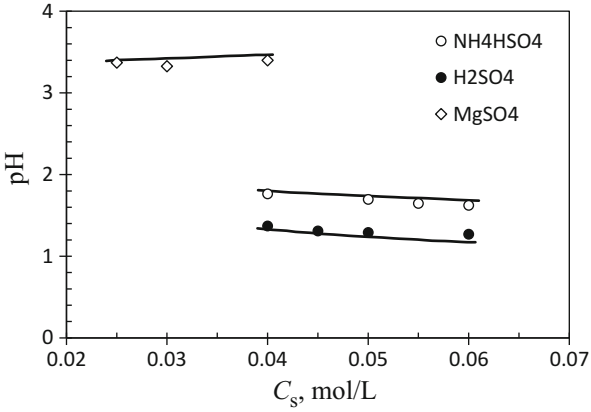

Fig. 3 Comparison between the measured (*symbols*) and predicted (*solid curves*) pH values for a fluorinated elastomer latex as a function of the salt concentration, for three types of salt, NH_4HSO_4, H_2SO_4, and $MgSO_4$, at particle volume fraction $\phi = 5.0 \times 10^{-3}$ [8]

H^+ to form HSO_4^-, the system pH increases slightly as the concentration of $MgSO_4$ increases. The capture of these slight variation trends confirms the reliability of the generalized stability model.

The second verification of model reliability is to predict the CCC value. This signifies using the generalized stability model, whose parameters were estimated at low salt concentrations, to extrapolate its application to substantially larger salt concentrations.

The CCC values are experimentally determined based on the fact that when diffusion-limited aggregation occurs at $\phi > 1 \times 10^{-3}$, clearly visible large pieces of clusters are formed immediately [35, 36]. Therefore, a given amount of latex was added to a series of salt concentrations to reach $\phi = 5 \times 10^{-3}$, and the time for the appearance of large clusters was recorded. The CCC value was obtained by extrapolation to the salt concentration at which the large clusters appear at time zero. Table 2 compares the measured CCC values of the three salts with the predicted values for three types of latexes. It should be mentioned that each predicted CCC value is reported with its significant error bar, because near the CCC the interaction energy barrier reduces asymptotically without a sharp change. It is clear that the model predictions are in good agreement with experimental results. Note that of the three latexes mentioned in Table 2, latex 1 is the one used above to define the generalized stability model; latexes 2 and 3 are similar to latex 1 but differ in the particle size and amount of surfactant. Thus, the model developed from latex 1 should be applicable to the other two cases. It is worth mentioning that since latexes 2 and 3 use less surfactant (i.e., smaller surface charge densities), both the measured and predicted CCC values are smaller than those of latex 1.

Table 2 Comparison between measured and predicted CCC values for three different salts used for fast coagulation of three latexes [8]

	CCC (mol/L)					
	H_2SO_4		NH_4HSO_4		$MgSO_4$	
Latex type	Exp.	Model	Exp.	Model	Exp.	Model
Latex 1	0.4	0.35 ± 0.05	0.52	0.55 ± 0.05	0.6	0.45 ± 0.05
Latex 2	0.3	0.25 ± 0.05	0.4	0.35 ± 0.05	–	–
Latex 3	0.3	0.25 ± 0.05	0.4	0.35 ± 0.05	–	–

3.2 Styrene–Acrylate Copolymer Latex with Both Mobile and Fixed Charges [37]

The second polymer colloid used to verify the generalized stability model was a styrene-acrylate copolymer latex, manufactured by BASF SE (Ludwigshafen, Germany) through emulsion polymerization with a carboxylate surfactant. Unlike the previous latex, this latex possesses fixed charges, $-SO_4^-$, on the particle surface as a result of the use of a persulfate initiator. Because it is stabilized by both mobile and fixed charges, we can compare its stability behavior to that investigated above with only mobile charges. The radius of primary particles is $a = 52$ nm, and the stability behavior is investigated at a fixed particle volume fraction, $\phi = 0.02$.

3.2.1 Estimation of the Model Parameters

To estimate the model parameters, we used the measured CCC values as a function of the system pH, using a bivalent salt, $MgSO_4$. The data were obtained using a similar method to that described above and are reported in Fig. 4. Note that because the pH of the original latex was 8.3, the pH value is tuned by adding H_2SO_4.

Considering $MgSO_4$ and H_2SO_4 as well as the mobile and fixed charges, we have three anions in the system, SO_4^{2-} and $-COO^-$ from the surfactant (denoted by E^-), and $-SO_4^-$ from the fixed charges (denoted by L^-), and two cations, H^+ and Mg^{2+}. Thus, there are a total of six association equilibria. To reduce fitting parameters, we use association equilibrium constants for similar molecules but with shorter chain lengths. This does not introduce significant error because, for long carbon chain surfactants, the electronic effects are transferred through molecular bonds and are not felt beyond two to three carbon atoms [38]. Five of the six association constants were taken from the literature and are reported in Table 3 [30]. The only association constant of Mg^{2+} with fixed charge L^- ($-SO_4^-$), K_{MgL^+}, was used as a fitting parameter, because of unavailability in the literature. We again used the Langmuir isotherm for surfactant adsorption, and of the two parameters, Γ_∞ and b, we assumed that Γ_∞ is equal to that of stearic acid on butadiene-styrene polymer particles, a system very similar to the present one [39], while b was used as a fitting parameter. The Hamaker constant, A_H, was estimated using the Lifshitz theory

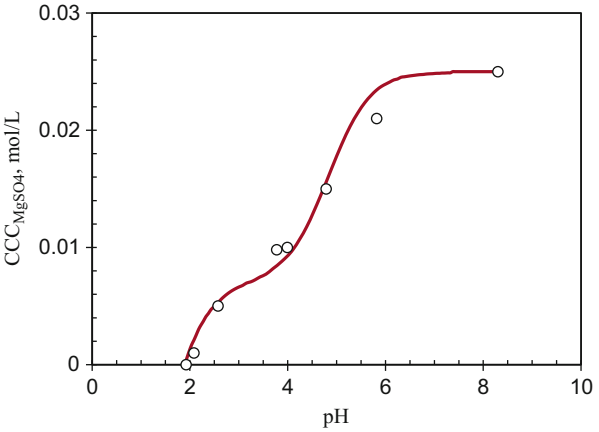

Fig. 4 CCC values (*symbols*) for $MgSO_4$ as a function of the system pH for a styrene-acrylate copolymer latex at ϕ=0.02; the *continuous curve* is the model simulation [37]

Table 3 Values of parameters for the generalized stability model in the case of styrene-acrylate copolymer latex [37]

Parameter		Cation (M)	
		H^+	Mg^{2+}
Association constants	K_{ME} (L/mol)	6.3×10^{4}[b]	3.5[b]
	K_{ML} (L/mol)	33.9[b]	2.5[a]
	K_{MSO_4} (L/mol)	97.0[b]	28.8[a]
Fixed charge amount	C_L (mol/m^3 polymer)	4.66[a]	
Hamaker constant	A_H (10^{-20} J)	1.3[d]	
Adsorption parameters	Γ_∞ (10^{-6} mol/m^2)	7.1[c]	
	b (10^3 L/mol)	0.88[a]	

[a]Fitted values
[b]Value taken from [30]
[c]Value taken from [39]
[d]Value computed from Lifshitz theory

[16]. The concentration of fixed charge groups C_L on the particle surface was used as a fitting parameter. Therefore, in total, there were three fitting parameters, K_{MgL^+}, b, and C_L, which were determined by fitting the nine CCC values at different pH values, as shown in Fig. 4.

It should be noted that for a small radius of the particles and the computed separation distance at the potential barrier larger than or close to 1 nm, we use the classical DLVO model for colloidal interactions and ignore any short-range non-DLVO forces. The simulated CCC values are compared with the experimental values in Fig. 4, and it is seen that not only the trend but also the absolute values are in good agreement. The values of the three fitted parameters, together with the values of the other parameters, as taken from the literature, are listed in Table 3.

3.2.2 Model Predictions and Applications

Both the experimental and simulated CCC data in Fig. 4 show two distinct regimes: one for pH $>$ 4 and another for pH $<$ 4. This corresponds to two types of surface charge, mobile $-COO^-$ (E^-) and fixed $-SO_4^-$ (L^-), as a result of their substantially different association constants with H^+, as reported in Table 3. Let us now manifest the system behavior by applying the generalized stability model to detail the surface charge concentrations on the particle surface as a function of pH.

Let us first consider the case in the absence of $MgSO_4$. The computed concentrations of mobile and fixed charge groups on the particle surface as a function of pH are given in Fig. 5a, and the corresponding total surface charge density (σ_0) and potential (ψ_0) are shown in Fig. 5b. It can be seen that at the original pH of the latex (8.3), because $E^- = E_{total}$ on the surface and L^- is at plateau, all the mobile and fixed charge groups on the surface are in dissociated form (E^- and L^-). The σ_0 and ψ_0 values in Fig. 5b reach their maximum (in absolute value) corresponding to the highest colloidal stability of the latex. In this case, the total surfactant concentration (E_{total}) on the surface is only composed of the dissociated anions, E^-. It is particularly important to mention that the E_{total} values on the surface and in the disperse medium are 8.16×10^{-3} mol/L and 2.54×10^{-4} mol/L, respectively, and do not follow the partitioning computed by the adsorption isotherm. The latter gives E_{total} values on the surface and in the disperse medium of 1.11×10^{-1} and 4.2×10^{-4} mol/L, respectively. This arises because the ionized E^- follows the Boltzmann distribution, resulting in its concentration at the particle–liquid interface being smaller than that in the bulk disperse medium. Because, for the generalized stability model, the surfactant adsorption equilibrium is considered to establish at the particle–liquid interface, the Boltzmann distribution certainly changes the amount of surfactant adsorbed on the particle surface (in fact, it is reduced because the ionic surfactant species are dominated by E^-). For pH $>$ 7.0, no significant changes occur, as shown in Fig. 5.

When the system pH is less than seven, the protonation process starts. Because $-COO^-$ (E^-) has a much larger association constant with H^+ than the fixed $-SO_4^-$ (L^-), its protonation initially dominates and follows that shown in Fig. 5a. The E^- concentration decreases sharply as pH decreases, while the fixed charge L^- concentration remains nearly constant. The decrease in σ_0 or $\psi_0$with decreasing pH in Fig. 5b is a result of a reduction in the mobile charges E^-. In the pH range between 3 and 4, the system reaches another (almost) flat region, where the E^- protonation is close to completion but the H^+ concentration is still insufficient to significantly protonate L^-. When the pH is less than three, L^- starts to protonate and its concentration decreases as pH decreases, as shown in Fig. 5a. This leads to sharper decreases in σ_0 and ψ_0 with decreasing pH. In this region, basically all E is in the protonated form, HE, and because HE does not follow the Boltzmann distribution, the partitioning of HE on the surface and in the bulk disperse medium is exactly given by the surfactant adsorption isotherm. Therefore, E_{total} is equal to HE on the particle surface and reaches a plateau. Referring back to Fig. 4, showing the

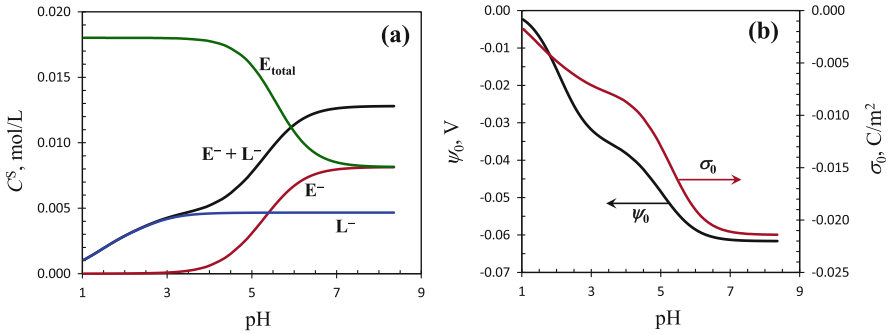

Fig. 5 Concentrations of charge groups E^- and L^- on the particle surface (**a**), and surface charge density σ_0 and potential ψ_0 (**b**), as a function of pH for the styrene-acrylate copolymer latex at $\phi = 0.02$ and $C_{MgSO_4} = 0$ [37]

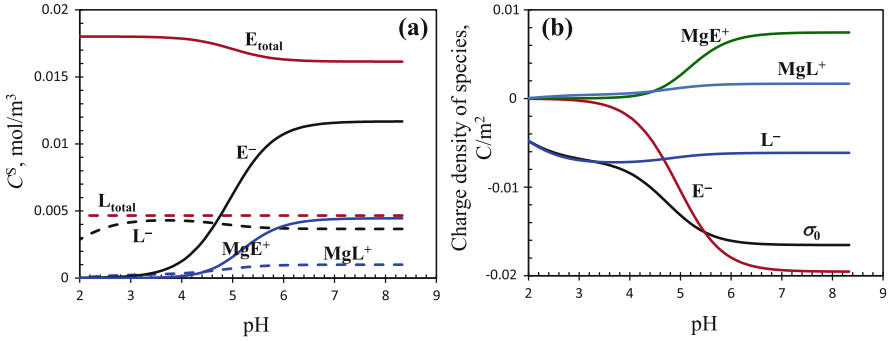

Fig. 6 (**a**) Concentrations of the surfactant, E, species (*solid curves*) and the fixed charge, L, (*broken curves*) groups on the particle surface, and (**b**) total and species charge densities as a function of the system pH, for the styrene-acrylate copolymer latex at $\phi = 0.02$ and $C_{MgSO_4} =$ 0.01 mol/L [37]

behavior of CCC values for $MgSO_4$, it is clear that for pH > 4, the change in CCC value with pH is related to protonation of the mobile charges, E^-; for pH < 4, it is due to protonation of the fixed charges, L^-.

For the presence of $MgSO_4$ at 0.01 mol/L, Fig. 6a shows the computed concentrations of the surfactant and fixed charge species on the particle surface as a function of pH. The total surface charge density (σ_0) and the contribution of each surface charge group are given in Fig. 6b.

Comparing Fig. 6a to Fig. 5a in the absence of Mg^{2+}, we see that the concentration variations of the surfactant species are very similar, but now the new species, MgE^+, is present on the surface as a result of E^-–Mg^{2+} association. In the presence of Mg^{2+}, the plateau value of the total surface charge density, σ_0 in Fig. 6c for pH > 7, is substantially smaller than that in Fig. 5b in the absence of Mg^{2+}. As the system pH decreases to less than seven, the surface concentrations of both E^- and Mg^{2+} species decrease. For E^-, this arises because of its protonation (as discussed

above), whereas for Mg^{2+}, we should consider that MgE^+ is progressively substituted by HE as pH decreases, because $-COO^-$ association with H^+ is much stronger than with Mg^{2+}.

For the species related to the fixed charge (L) groups, their concentration variations shown in Fig. 6a differ from those in Fig. 5a, as a result of the presence of Mg^{2+}. The L^- concentration in Fig. 6a increases as pH decreases, and then decreases after reaching a local maximum at around pH ~ 3.5. However, as shown in Fig. 5a, there is no such local maximum in the L^- concentration in the absence of Mg^{2+}. To explain this, we should recall that the total amount of fixed charge groups (L_{total}) is constant, which is a sum of L^- and MgL^+ in Fig. 6a. As pH decreases by adding H_2SO_4, the ionic strength increases, leading to a decrease in the surface potential. The latter, through the effects of Boltzmann distribution, results in a shift of positive Mg^{2+} ions from the particle–liquid interface to the liquid phase, thus favoring the dissociation of MgL^+ on the surface and freeing more L^-. Consequently, the L^- concentration increases as pH decreases for pH $>$ 3.5 (Fig. 6a). In the region of pH $<$ 3.5, protonation of the L^- species becomes dominant, and it follows that the L^- concentration starts to decreases with decreasing pH.

3.3 Butylacrylate-Methylmethacrylate-Acrylic Acid Copolymer Latexes

The third type of polymer colloids used here for verifying the model feasibility is represented by two butylacrylate-mehthylmethacrylate-acrylic acid copolymer latexes, referred to as P1 and P2. They were supplied by BASF SE (Ludwigshafen, Germany), produced through emulsion polymerization with $Na_2S_2O_8$ as initiator and sodium dodecyl sulfate (SDS) as emulsifier. The radius of the particles is 80.0 and 81.0 nm, respectively, for P1 and P2. The main difference between them is the amount of acrylic acid (AA) used in the polymerization, which is 0% for P1 and 1% for P2. It follows that the particles of P1 possess only the fixed charges $-SO_4^-$ and those of P2 contain both $-SO_4^-$ and $-COO^-$ (fixed) charges. The SDS surfactant was removed completely using ion exchange resins [40]. Therefore, after cleaning, unlike the latexes described in Sects. 3.1 and 3.2, the P1 and P2 latexes possess only fixed charges. It should be pointed out that P1 and P2 latexes (after removing the surfactant used during polymerization) represent the simplest type of polymer colloid. Similar but different systems have also been used to successfully verify the generalized stability model [41].

3.3.1 P1 Latex with Only Sulfate Groups

For the P1 latex, the W values measured in the presence of NaCl and H_2SO_4 are reproduced from the literature [42] and shown in Fig. 7a. The corresponding pH

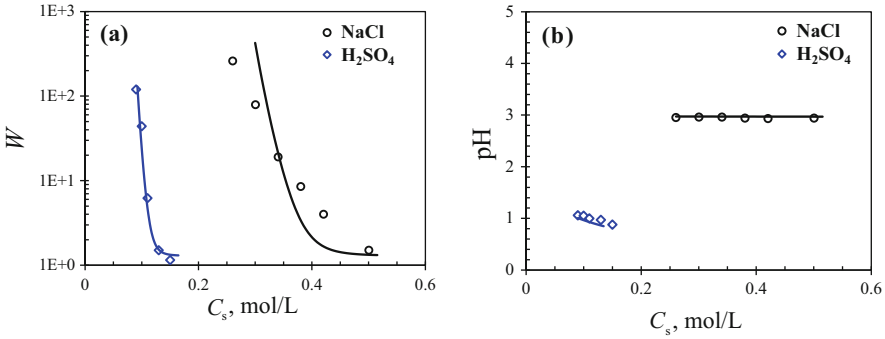

Fig. 7 Comparison between measured (*symbols*) and simulated (*solid curves*) values for (**a**) the Fuchs stability ratio W and (**b**) pH values, for P1 latex at $\phi = 2.0 \times 10^{-5}$, destabilized by NaCl and H_2SO_4

values are reported in Fig. 7b. Because P1 possesses only the fixed charges $-SO_4^-$ (denoted by I) on the particle surface, it is the simplest latex considered. For P1, we have a total of seven parameters: A_H, $C_{I,T}^S$, K_{HI}, K_{NaI}, $F_{0,H}$, $F_{0,Na}$, and δ_0. Of these, values for $A_H(1.0 \times 10^{-20}$ J) and δ_0 (0.40 nm) are taken from the literature. For the total concentration of $-SO_4^-$ on the particle surface, $C_{I,T}^S$, we used the result obtained previously [37] (i.e., with respect to the total added initiator during the polymerization) that 33.1% $-SO_4^-$ groups remain on the particle surface. From the polymerization recipe, this corresponds to $C_{I,T}^S = 0.0235$ mol/kg polymer. The remaining four parameters, K_{HI}, K_{NaI}, $F_{0,H}$, and $F_{0,Na}$, are used as fitting parameters. In addition, because H_2SO_4 was used to destabilize the latex and tune pH, there are two associations of SO_4^{2-} in the bulk disperse medium with H^+ and Na^+. Equilibrium constants $K_{HSO_4^-}$ and $K_{NaSO_4^-}$ were taken directly from the literature [30], being equal to 97.0 and 5.0 L/mol, respectively.

Following the same procedure as above, the simulated values of two sets of W values are shown in Fig. 7a, as well as the corresponding pH values in Fig. 7b. All the simulations are very satisfactory, but in the case of NaCl, the simulations show significantly sharper decrease in the W value with C_S than the experimental data. This could indicate that the hydration interaction increases as more Na^+ ions are associated on the surface. The obtained values for the unknown parameters are listed in Table 4 under P1. The obtained value for K_{HI} is about one order of magnitude larger than that for K_{NaI}, which follows the same trend as $K_{HSO_4^-}$ with respect to $K_{NaSO_4^-}$. Both K_{HI} and K_{NaI} values are substantially smaller than those of $K_{HSO_4^-}$ and $K_{NaSO_4^-}$. The obtained K_{HI} value is equal to 33.1 L/mol, which is comparable to the association constant of propyl sulfonate ($C_3H_7SO_3^-$) with H^+ [30], but smaller. In fact, the association constant of SO_4^{2-} with H^+ is also smaller than that of SO_3^{2-} with H^+. The estimated values for the hydration force constants, $F_{0,H}$ and $F_{0,Na}$ for P1, are well within the range reported in the literature (1×10^6–5×10^8 N/m^2). Note that $F_{0,H}$ and $F_{0,Na}$ were considered to be independent of the salt concentration. The $F_{0,H}$ value is smaller than the $F_{0,Na}$ value, indicating that the

Table 4 Values of the parameters for P1 and P2 latexes obtained from fitting the measured W values

Latex	K_{HI} (L/mol)	K_{NaI} (L/mol)	$F_{0,H}$ (N/m^2)	$F_{0,Na}$ (N/m^2)	$C^s_{L,T}$ (mol/kg P)	K_{HL} (L/mol)	K_{NaL} (L/mol)
P1	16.0	1.80	7.77×10^6	8.80×10^6	–	–	–
P2	16.0	1.80	12.1×10^6	(in Fig. 10)	0.0866	4.0×10^6	2.80

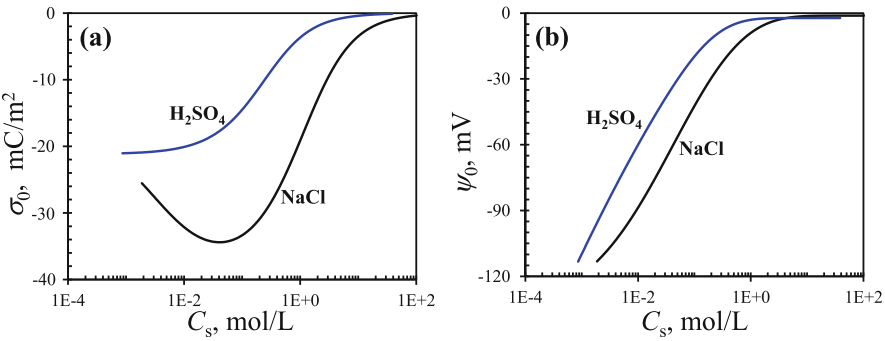

Fig. 8 Surface charge density σ_0 and surface potential ψ_0 computed from the generalized stability model using the estimated parameters in Table 4, for P1 latex at $\phi = 2.0 \times 10^{-5}$, destabilized by NaCl and H_2SO_4

hydration force in the presence of H_2SO_4 is smaller than that in the presence of NaCl. Such a trend is consistent with those reported in the literature [8, 43].

With estimated values for all the model parameters, the generalized stability model has been well established for P1 latex and can be applied to analysis of the system stability. As examples, let us calculate the evolutions of the surface charge density (σ_0) and potential (ψ_0) with salt concentration, which in most cases are difficult to determine experimentally. Figure 8a, b shows the computed σ_0 and ψ_0 values as functions of the salt (NaCl or H_2SO_4) concentration. In the case of H_2SO_4, both σ_0 and ψ_0 (absolute values) decrease as the H_2SO_4 concentration increases. For σ_0, this arises because of association of added H^+ with the surface $-SO_4^-$ charge groups. For ψ_0, the decrease is the result of two factors: (1) σ_0 reduction and (2) the screening effect of an increase in ionic strength.

For NaCl as destabilizer, the variation in surface charge density σ_0 with NaCl concentration C_S in Fig. 8a is rather peculiar. At low C_S, the absolute σ_0 value increases as C_S increases, instead of decreasing. Only when the σ_0 value reaches a local maximum at around $C_S = 0.04$ mol/L, does it start to decrease with C_S. It is worth pointing out that, without the generalized stability model, such behavior would be very difficult to observe experimentally. To explain the observed phenomenon, we should first consider that the surface charge results from the association equilibria between the surface $-SO_4^-$ groups and cations Na^+ and H^+ at the particle–liquid interface. As the NaCl concentration increases, the increased Na^+ ions at the interface in principle drive the equilibrium towards association, thus

decreasing the surface charge; however, the computed surface charge increases, which means that the increased Na^+ concentration in the bulk disperse medium leads to a decrease (rather than an increase) in the Na^+ concentration at the particle–liquid interface. The occurrence of this phenomenon is related to the Boltzmann equation:

$$C_j^i = C_j^b \exp\left(-\frac{z_j e\psi_0}{kT}\right) \tag{20}$$

Indeed, the concentration at the interface, C_j^i, increases as the concentration in the bulk disperse medium,C_j^b, increases (from Eq. 20), but the increase in C_j^b also leads to a decrease in the surface potential (ψ_0) as a result of the screening effect. Then, the exponent term in Eq. (20) decreases with C_j^b. Thus, whether C_j^i increases or decreases with C_j^b depends on the combined effect of C_j^b and the exponent term. As can be seen in Fig. 8a, at NaCl concentrations smaller than about 0.04 mol/L the absolute ψ_0 value is very large, and variations in ψ_0 result in substantial changes in the value of the exponent term. Thus, the effect of the exponent term overwhelms that of C_j^b, leading to C_j^i decreasing with C_j^b. It follows that σ_0 increases with the NaCl concentration. With further decrease in ψ_0, because its value is small, the effect of the exponent term becomes smaller than that of C_j^b, and C_j^i increases with C_j^b, leading to a decrease in σ_0.

3.3.2 P2 Latex with 1% PAA

On the particle surface of P2 latex, apart from the fixed $-SO_4^-$ groups, there are also carboxylic groups from PAA formed from 1% acrylic acid monomer, which when ionized (–COO^-) contribute to the surface charge. The measured W values at different pH values in the presence of NaCl and H_2SO_4, respectively, are reproduced from previous work [42] and shown in Fig. 9a; the corresponding pH values are reported in Fig. 9b. The contributions of 1% PAA to the colloidal stability can be modeled by simulating the W and pH values using the generalized stability model. Except for 1% AA, the recipe for P2 is basically the same as that for P1. Thus, to reduce the fitting parameters, we assume that the total $-SO_4^-$ concentration on the particle surface is identical for P1 and P2. Then, the values for the parameters $C_{I,T}^S$, K_{HI} and K_{NaI} evaluated for P1 (Table 4) can be directly used for P2. Because of the presence of $-COO^-$ groups on the surface, whose properties depend strongly on pH, we expect that the hydration force constants, $F_{0,H}$ and $F_{0,Na}$, also vary with pH. Thus, they are still set as fitting parameters.

There are three parameters related to the $-COO^-$ groups: the total carboxylic group contraction on the surface, $C_{L,T}^S$, and two association constants of $-COO^-$ with H^+ and Na^+, K_{HL} and K_{NaL}, respectively. The $C_{L,T}^S$ value has been determined by titration and is equal to 0.0866 mol/kgP, as given in Table 4 under P2. Therefore, for P2, we have a total of four fitting parameters, $F_{0,H}$, $F_{0,Na}$, K_{HL}, and K_{NaL}, to be

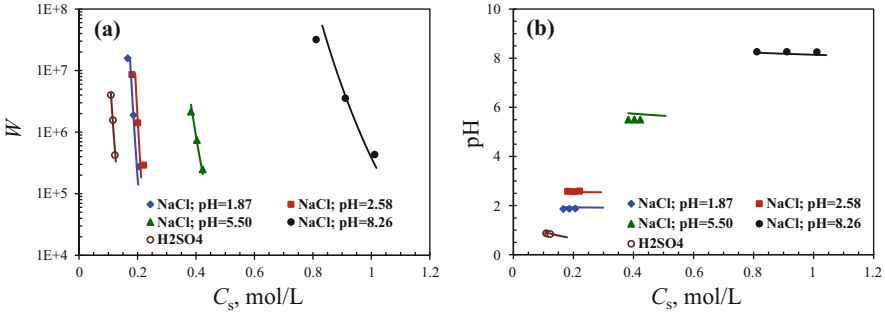

Fig. 9 Comparison between measured (*symbols*) and simulated (*solid curves*) values of (**a**) the Fuchs stability ratio W and (**b**) pH values, for P2 latex at $\phi = 5.0 \times 10^{-2}$, destabilized by NaCl and H_2SO_4

determined from simulations of W and pH values. The simulation results are shown in Fig. 9 a, b, and we can see that the agreement between experiments and simulations is very satisfactory. The obtained values for all the unknown parameters are reported in Table 4 under P2.

Let us first analyze the simulation results for W and pH corresponding to H_2SO_4, which involve only two fitting parameters, K_{HL} and $F_{0,H}$. It is seen in Fig. 9 that the three W and three pH values have been excellently simulated. However, the obtained association constant of $-COO^-$ with H^+ (K_{HL} in Table 4), is unreasonably large, equal to 4.0×10^6 L/mol, which is almost two orders of magnitude larger than the typical value of 2×10^4–6.3×10^4 L/mol for the association of $-COO^-$ with H^+ when $-COO^-$ is present at the end of a polymer chain [30, 37, 41]. Such an extremely large K_{HL} value indicates that the consumption of H^+ ions is more than the association equilibrium requires. We believe that this is a consequence of the presence of PAA chains, which are in the collapsed state in the H_2SO_4 solution. The protonated carboxylic groups ($-COOH$) are buried in the collapsed layer and do not participate in the association equilibrium. Because this protonated "dead" $-COOH$ state consumes a lot of H^+ ions, one has to increase the K_{HL} value to compensate for the consumed H^+ in order to fit the measured pH values. The hydration force constant $F_{0,H}$ in the presence of H_2SO_4 is much larger for P2 than for P1 (as shown in Table 4), signifying that even in the collapsed state at such low pH, the PAA brushes lead to an increase in surface hydrophilicity as a result of the polar nature of carboxylic acid.

Using NaCl as destabilizer, because the W values in Fig. 9 were measured at different pH values (tuned using H_2SO_4), the association of $-COO^-$ with H^+ is also involved. In the simulations, we directly applied the value for the association constant of $-COO^-$ with H^+, K_{HL}, obtained in the case where H_2SO_4 was used as destabilizer. Thus, we have only two fitting parameters, $F_{0,Na}$ and K_{NaL}. The obtained value for K_{NaL}, the association constant of $-COO^-$ with Na^+, is equal to 2.80 L/mol (Table 4). This value is comparable with the value of 2.65 L/mol estimated for perfluoropolyether-based carboxylic groups in another work [8]. It

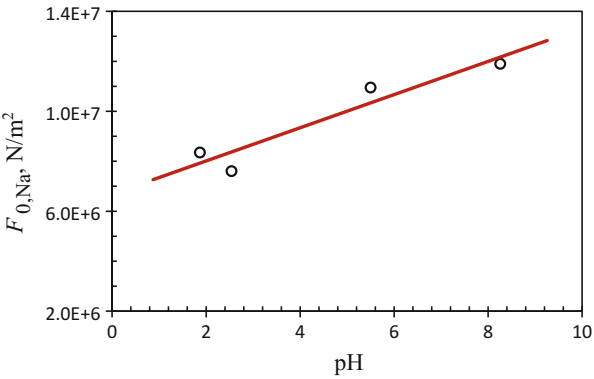

Fig. 10 Hydration force constant $F_{0,\mathrm{Na}}$ for P2 latex as a function of pH, estimated from W simulations using NaCl as the destabilizer at $\phi = 5.0 \times 10^{-2}$

is interesting to see that the estimated value for the hydration force constant, $F_{0,\mathrm{Na}}$ as shown in Fig. 10, increases as pH increases. This indicates that, as pH increases, more carboxylic groups are deprotonated and the surface becomes more polar (i.e., more hydrophilic). However, such an explanation is inconsistent with the results of previous work [41], where we simulated the W values of a colloidal system stabilized by fixed carboxylic groups, but not PAA (previously measured at pH 3–10 by Behrens et al. [44]). It was found that, using the generalized stability model accounting for only the DLVO colloidal interactions, we can describe the system stability behavior in the entire range of pH 3–10, without even introducing the hydration force. This means that carboxylic acid when deprotonated acts mainly as a charge group contributing to electrostatic repulsion, and that its contribution to the hydration force is not substantial. Thus, the increase in $F_{0,\mathrm{Na}}$ with pH (Fig. 10) cannot be explained by the hydration force. Instead, we believe that this results from the steric force of the PAA chains, which, as pH increases, become more stretched and contribute more and more to particle stability. Because steric interactions are not included in our model, they are naturally lumped into the hydration force, leading to an increase in $F_{0,\mathrm{Na}}$ with pH.

Based on the above discussion, we can explain why the $F_{0,\mathrm{H}}$ value at very low pH (<1) in Table 4 is larger than the $F_{0,\mathrm{Na}}$ values at pH ~ 2 in Fig. 10 by considering that the protonated $-$COOH contributes to the hydration force, but the deprotonated $-\mathrm{COO}^-$ does not. At pH 2, the amount of $-$COOH is reduced and the hydration force is reduced. Of course, the increase in deprotonated $-\mathrm{COO}^-$ (as well as $-\mathrm{SO}_4^-$) groups contributes to electrostatic repulsion, which has a dominant effect on W. In fact, the W values in the case of NaCl at pH 1.87 and 2.58 are larger than those for H_2SO_4 at pH < 1 (Fig. 9a).

Using the established generalized stability model, we calculated the surface charge density and potential (σ_0 and ψ_0) as functions of the concentration of total added salts (H_2SO_4 + NaCl), C_s. The conditions corresponded to those for the five sets of experiments shown in Fig. 9a, b, and the results are shown in Fig. 11a, b. It is seen that for pH < 3, the variations in σ_0 and ψ_0 with C_s in Fig. 11b are very similar to those in Fig. 8a, b for P1 latex. This is because at low pH most of the $-\mathrm{COO}^-$

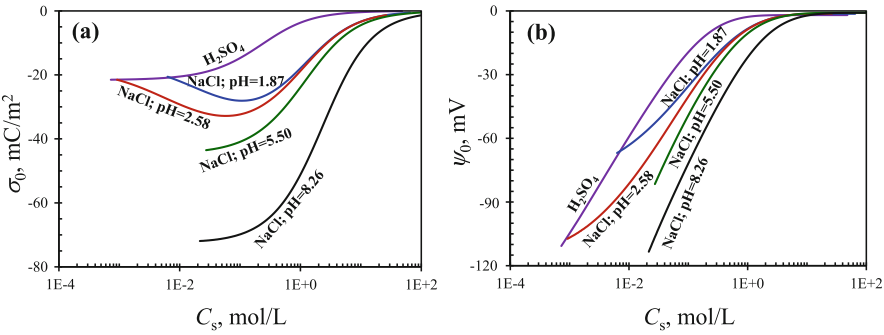

Fig. 11 Surface charge density σ_0 and surface potential ψ_0 computed from the generalized stability model using the estimated parameters in Table 4, for P2 latex at $\phi = 5.0 \times 10^{-2}$, destabilized by NaCl and H_2SO_4

groups are protonated and the surface charge mainly comes from $-SO_4^-$, which is practically the same for P1 and P2 latexes. As pH increases, the surface charge density and potential increase as a result of the increase in $-COO^-$ groups.

4 Concluding Remarks

We have reviewed the generalized stability model developed in recent years [8] and particularly its application to various polymer colloids. The stability of a colloidal system is not only determined by the DLVO colloidal interactions but is also affected by the interplay of other physicochemical processes such as surfactant adsorption equilibrium on the particle surface, association equilibria of the surface charges with counterions involved in the system, and non-DLVO colloidal interactions. The generalized stability model can account simultaneously for such complex interplay between different processes. The model has been successfully validated through its application to different polymer colloids produced from industrial polymerization processes, and its powerful capacity to describe the stability of complicated colloidal systems demonstrated.

Various processes are involved in the model and therefore the model parameters need to be defined. The values of some of the parameters are reported in the literature, and values for the remaining unknown parameters are required. We propose that their values be estimated through application of the model to fit ad hoc experiments, such as the value of the Fuchs stability ratio as a function of salt concentration, the CCC values of different types of salts, etc. Once all the parameters are defined, the established model can be used to analyze in detail how the interplay between different processes affects the stability of the system.

From application of the generalized stability model to different polymer colloids, we have demonstrated that the interplay between various physicochemical processes is substantial. Such interplay can result in very different (peaked or

monotonic) tendencies of the surface charge density and different surfactant partitioning between the particle surface and the bulk disperse medium, with respect to changes in the ionic strength, counterion type, pH, etc. Therefore, the generalized stability model can be used as a reliable tool for understanding and defining suitable conditions for obtaining the desired stability during the production and application of polymer colloids for both industrial practice and academic purpose.

Acknowledgements Financial support from the Swiss National Science Foundation (Grant No. 200020_165917) is gratefully acknowledged.

References

1. Isrealachvili JN (1991) Intermolecular and surface forces, 2nd edn. Academic, London
2. Hunter RJ (2001) Foundations of colloid science. Oxford University Press, New York
3. Ninham BW, Yaminsky V (1997) Ion binding and ion specificity: the Hofmeister effect and Onsager and Lifshitz theories. Langmuir 13:2097–2108
4. Ruckenstein E, Manciu M (2003) Specific ion effects via ion hydration: II. Double layer interaction. Adv Colloid Interf Sci 105:177–200
5. Kunz W, Lo Nostro P, Ninham BW (2004) The present state of affairs with Hofmeister effects. Curr Opin Colloid Interface Sci 9:1
6. Manciu M, Ruckenstein E (2004) The polarization model for hydration/double layer interactions: the role of the electrolyte ions. Adv Colloid Interf Sci 112:109
7. Parsegian VA, Zemb T (2011) Hydration forces: observations, explanations, expectations, questions. Curr Opin Colloid Interface Sci 16:618–624
8. Jia ZC, Gauer C, Wu H, Morbidelli M, Chittofrati A, Apostolo M (2006) A generalized model for the stability of polymer colloids. J Colloid Interface Sci 302:187–202
9. Leikin S, Parsegian VA, Rau DC, Rand RP (1993) Hydration forces. Annu Rev Phys Chem 44:369–395
10. Grahame DC (1947) The electrical double layer and the theory of electrocapillarity. Chem Rev 41:441–501
11. Bloch JM, Yun W (1990) Condensation of monovalent and divalent metal ions on a Langmuir monolayer. Phys Rev A 41:844
12. Lucassen-Reynders EH (1981) Anionic surfactants: physical chemistry of surfactant action. Marcel Dekker, New York
13. Zhu B-Y, Gu T (1991) Surfactant adsorption at solid-liquid interfaces. Adv Colloid Interf Sci 37:1–32
14. Mclaughlin S, Mulrine N, Gresalfi T, Vaio G, Mclaughlin A (1981) Adsorption of divalent cations to bilayer membranes containing phosphatidylserine. J Gen Physiol 77:445–473
15. Koopal LK, Goloub T, De Keizer A, Sidorova MP (1999) The effect of cationic surfactants on wetting colloid stability and flotation of silica. Colloid Surf A Physicochem Eng Asp 151:15–25
16. Israelachvili JN (2011) Intermolecular and surface forces, 3rd edn. Academic Press, San Diego
17. Faraudo J, Bresme F (2005) Origin of the short-range, strong repulsive force between ionic surfactant layers. Phys Rev Lett 94:077802
18. Boström M, Williams DRM, Ninham BW (2001) Specific ion effects: why DLVO theory fails for biology and colloid systems. Phys Rev Lett 87:168103

19. Valle-Delgado JJ, Molina-Bolivar JA, Galisteo-Gonzalez F, Galvez-Ruiz MJ, Feiler A, Rutland MW (2005) Hydration forces between silica surfaces: experimental data and predictions from different theories. J Chem Phys 123(3):034708
20. Sader JE, Carnie SL, Chan DYC (1995) Accurate analytic formulas for the double-layer interaction between spheres. J Colloid Interface Sci 171:46–54
21. Runkana V, Somasundaran P, Kapur PC (2005) Reaction-limited aggregation in presence of short-range structural forces. AICHE J 51:1233–1245
22. Derjaguin VB (1934) Studies on friction and adhesion IV. Theory of adhering small particles. Kolloid-Z 69:155–164
23. Wu H, Tsoutsoura A, Lattuada M, Zaccone A, Morbidelli M (2010) Effect of temperature on high shear-induced gelation of charge-stabilized colloids without adding electrolytes. Langmuir 26:2761–2768
24. Spielman LA (1970) Viscous interactions in Brownian coagulation. J Colloid Interface Sci 33:562
25. Honig EP, Roebersen GJ, Wiersema PH (1971) Effect of hydrodynamic interaction on the coagulation rate of hydrophobic colloids. J Colloid Interface Sci 36:97
26. Manciu M, Ruckenstein E (2001) Role of the hydration force in the stability of colloids at high ionic strengths. Langmuir 17:7061–7070
27. Manciu M, Ruckenstein E (2003) Specific ion effects via ion hydration: I. Surface tension. Adv Colloid Interf Sci 105:63
28. Huang H, Manciu M, Ruckenstein E (2005) On the restabilization of protein-covered latex colloids at high ionic strengths. Langmuir 21:94–99
29. Sinha P, Szilagyi I, Montes Ruiz-Cabello FJ, Maroni P, Borkovec M (2013) Attractive forces between charged colloidal particles induced by multivalent ions revealed by confronting aggregation and direct force measurements. J Phys Chem Lett 4:648–652
30. Martell AE, Smith RM (1989) Critical stability constants. Plenum, New York
31. Maeda M, Iwata T (1997) Dissociation constants of ammonium ion and activity coefficients of ammonia in aqueous ammonium sulfate solutions. J Chem Eng Data 42:1216–1218
32. Chittofrati A (2005) Self-association of model perfluoroplyether carboxylic salts internal report. Solvay, Bollate
33. Thompson DW, Collins IR (1994) Electrolyte-induced aggregation of gold particles on solid surfaces. J Colloid Interface Sci 163:347–354
34. Evans DF, Wennerström H (1999) The colloidal domain: where physics, chemistry, biology, and technology meet, 2nd edn. Wiley-VCH, Weinheim
35. Lattuada M, Wu H, Sandkühler P, Sefcik J, Morbidelli M (2004) Modelling of aggregation kinetics of colloidal systems and its validation by light scattering measurements. Chem Eng Sci 59:1783
36. Wu H, Xie J-J, Morbidelli M (2005) Kinetics of cold-set diffusion-limited aggregations of denatured whey protein isolate colloids. Biomacromolecules 6:3189–3197
37. Jia ZC, Wu H, Morbidelli M (2007) Application of the generalized stability model to polymer colloids stabilized with both mobile and fixed charges. Ind Eng Chem Res 46:5357–5364
38. Fox MA, Whitesell JK (1997) Organic chemistry. Jones And Bartlett, Boston
39. Maron SH, Elder ME, Ulevitch IN (1954) Determination of surface area and particle size of synthetic latex by adsorption I. latices containing fatty acid soaps. J Colloid Sci 9:89
40. Zaccone A, Wu H, Lattuada M, Morbidelli M (2008) Correlation between colloidal stability and surfactant adsorption/association phenomena studied by light scattering. J Phys Chem B 112:1976–1986
41. Ehrl L, Jia ZC, Wu H, Lattuada M, Soos M, Morbidelli M (2009) Role of counterion association in colloidal stability. Langmuir 25:2696–2702
42. Jaquet B, Wei D, Reck B, Reinhold F, Zhang X, Wu H, Morbidelli M (2013) Stabilization of polymer colloid dispersions with ph-sensitive poly-acrylic acid brushes. Colloid Polym Sci 291:1659–1667

43. Pashley RM (1981) Hydration forces between mica surfaces in aqueous-electrolyte solutions. J Colloid Interface Sci 80:153–162
44. Behrens SH, Christl DI, Emmerzael R, Schurtenberger P, Borkovec M (2000) Charging and aggregation properties of carboxyl latex particles: experiments versus DLVO theory. Langmuir 16:2566–2575